Hindawi
International Journal of Rotating Machinery
Volume 2021, Article ID 6691128, 19 pages
https://doi.org/10.1155/2021/6691128

Research Article

Experimental Film Cooling Effectiveness of Three-Hole-Branch Circular Holes

Fan Yang and Mohammad E. Taslim

Mechanical and Industrial Engineering Department, Northeastern University, Boston, Massachusetts 02115, USA

Correspondence should be addressed to Mohammad E. Taslim; m.taslim@northeastern.edu

Received 26 October 2020; Revised 4 August 2021; Accepted 3 September 2021; Published 11 October 2021

Academic Editor: Terrence W. Simon

A three-hole-branch geometry for film cooling is proposed. Each branch is made up of a streamwise 30°-angled circular hole with a circular hole of the same diameter on each side of it. These three holes share the same inlet area on the coolant supply side. Three side hole inclination angles of 30°, 37.5°, and 45° and three branch angles (the angle between the main and side holes) generated nine configurations that were tested for four blowing ratios of 0.5, 1, 1.5, and 2. To their benefits, these straight-through circular holes could easily be laser drilled on the airfoils or other gas turbine hot section surfaces. For comparative evaluation of these film hole geometries, the commonly used 7°-7°-7° diffusion hole geometry with the same inlet hole diameter was tested as a baseline under otherwise identical conditions. The pressure-sensitive paint (PSP) technique was utilized to test these geometries for their film cooling effectiveness. Depending on the branch geometry, for the same amount of coolant, some configurations were found to be superior to the baseline case for stream- or spanwise film cooling distributions while for the steeper side hole angles, these branched holes did not perform as well as the baseline case. The main conclusion is that the three holes with the same inclination angle of 30° exhibited the best film cooling effectiveness performance including the baseline geometry.

1. Introduction

Gas turbines are widely used in the industry to provide power for electric generators, aircrafts, trains, and ships. To maximize the power output and improve the efficiency, the turbine inlet temperature has been consistently increased. However, the increasing high inlet temperature may cause elevated thermal loads on the components that will damage the turbine airfoils and other hot sections, which reduces the durability of the whole system. Several features are in use to protect the turbine hot sections. Airfoil designs in modern gas turbines may include rib-roughened cooling cavities, pin banks, impingement holes and inserts, film holes and slots, thermal barrier coatings, and other features for thermal protection against the combustor gases.

Cooling of the airfoil external surfaces is often accomplished by drilling film holes of various geometries at strategic spots on the airfoil surfaces. The ejected coolant creates a cooling blanket over the targeted surface. The main objective in designing the airfoil circuits, including the film cooling scheme, is gaining maximum coolant coverage with minimum spent air and minimum aerodynamic losses. Numerous research studies, experimental as well as numerical, encompassing many aspects of film cooling, including branched hole geometries, have been reported in the open literature over the past several decades.

To go over the details of each study is well beyond the allotted space in this manuscript. We, however, would like to refer the reader to the work of pioneers such as Goldstein et al. [1], Eriksen and Goldstein [2], and Pedersen et al. [3] in this field who investigated the effects of main parameters such as hole geometry, density ratio, and blowing ratio on three-dimensional film cooling. Bogard et al. [4] and Sen et al. [5] reported adiabatic film cooling effectiveness values

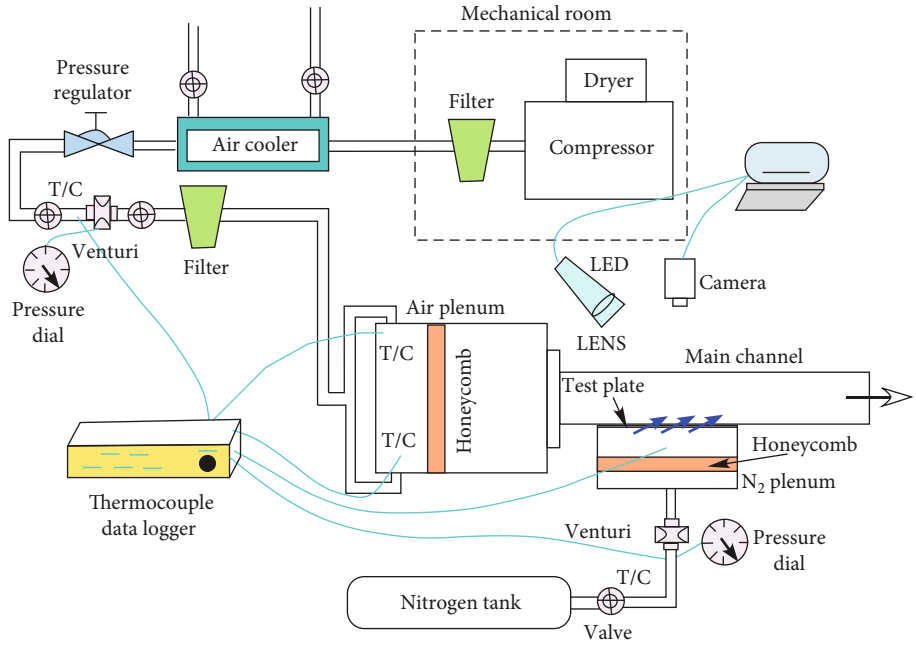

Figure 1: Test rig, associated accessories, and data collection equipment.

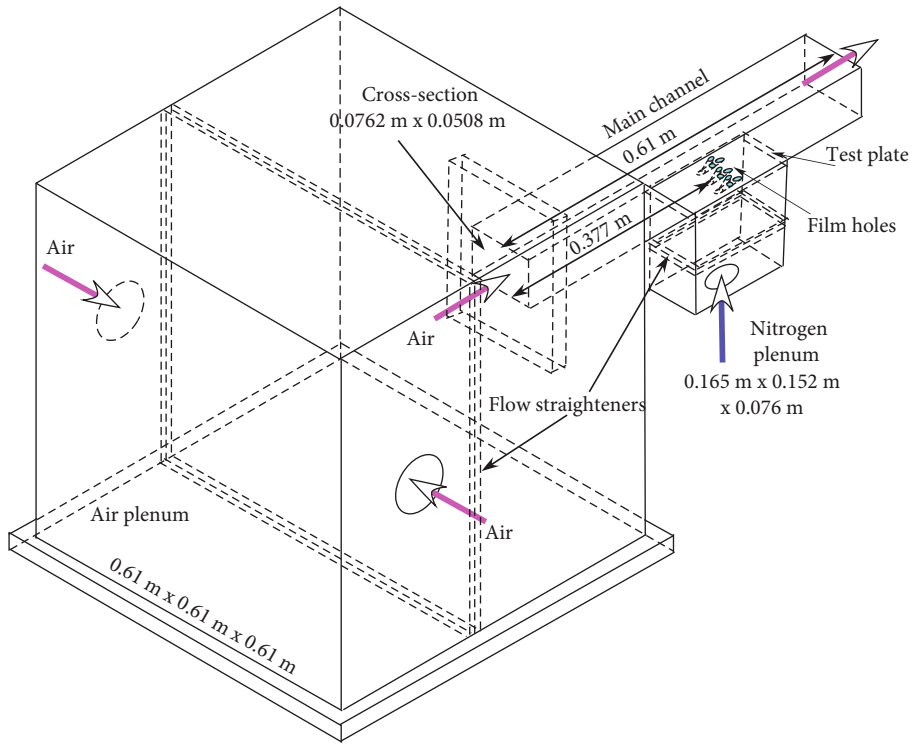

Figure 2: Schematic of the test rig.

and heat transfer coefficients downstream of compound angle holes. One major conclusion was that adding a compound angle to the baseline round hole geometry significantly improved film effectiveness at high momentum flux ratios, and the combination of compound angle and forward expansion provided further improvement. Bunker [6] presented a thorough review of shaped hole turbine film cooling technology. Among his conclusions were the

Table 1: Geometric parameters (lengths in mm).

d	P	P/d	L	L/d	ℓ	α_1	α_2	β_{fwd}	β_{lat}	D_h
3.81	22.86	6	22.86, 18.78, 16.16	6, 4.93, 4.24	9.53	30°	30°, 37.5°,45°	7°	7°	61

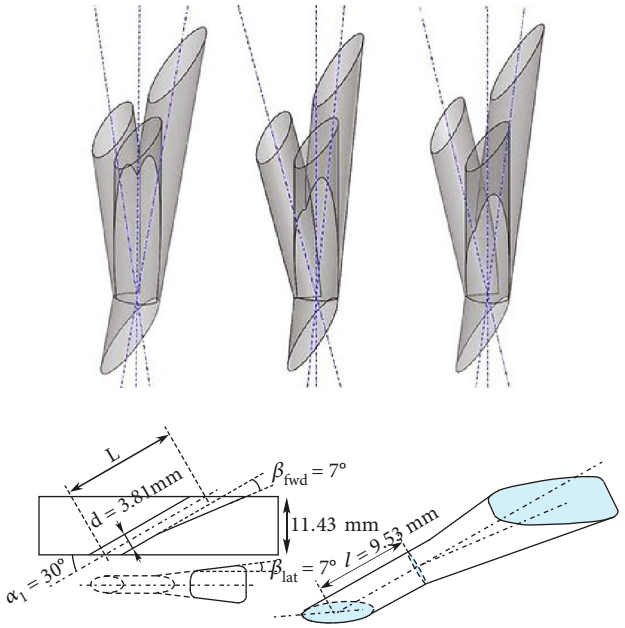

Figure 3: Schematics of the branched film hole geometries (top) and 7°-7°-7° diffusion hole baseline (bottom).

shaped holes outperformed the circular holes and the fact that as manufacturing methods progress, other unconventional shapes of film holes will become viable and could lead to even better performance and less cooling air requirements.

This paper focuses on the geometric parameters of the antivortex holes that can help improve the film cooling performance. Heidmann and Ekkad [7] reported a numerical study on a novel antivortex film hole geometry. Two side holes with half the diameter of the primary hole were angled in spanwise direction and normal to streamwise direction. The side holes provided a strong vortex against the detrimental vortices produced by the primary hole. They showed that the geometry with the side holes originating near the primary hole inlet improved the overall film cooling effectiveness. Dhungel et al. [8] continued the experimental study of this antivortex geometry by changing both the originating and ending locations of the side holes. The best result was achieved when the side hole ending locations were in line with the primary hole. Yao et al. [9] performed a numerical study on film cooling mechanisms and characteristics of cylindrical holes with branched jet injections. Their geometries were very similar to the previous study and could serve as a CFD complementary for comparisons. Repko et al. [10] confirmed the advantage of antivortex holes and used a similar geometry on their study of freestream turbulence levels. The sister-shaped single-hole geometry in the study of Khajehhasani and Jubran [11] was also a member of the antivortex family, but with the originating locations of the side holes at the ending location of the main hole. This geometry had remarkable performance in the distant downstream region at the high blowing ratios of 1 and 1.5.

Different from the studies above, the antivortex geometry in the current study is tripod shaped, with side holes' diameter and originating location the same as those of the primary hole. LeBlanc et al. [12] investigated, experimentally and numerically, the film cooling performance of an antivortex hole and a trenched antivortex hole on a flat plate. Their case (b), antivortex/tripod, hole was a typical shape with its side and main holes having the same diameter and inlet location. Ravi et al. [13] investigated the film cooling performance of tripod holes on the endwall upstream of a first-stage nozzle guide vane. Three geometries were tested: purge slot, cylindrical, and tripod holes. They concluded that slot ejection gave the highest effectiveness amongst the three tested configurations and the tripod holes outperformed the cylindrical holes. Ramesh et al. [14, 15] reported the film cooling effectiveness values of tripod antivortex injection holes over the pressure and suction surfaces of a nozzle guide using infrared thermography. They examined cylindrical, shaped, tripod, and shaped–tripod holes for a blowing ratio range of 0.5 to 4. Their major conclusions were that shaping improves the film cooling effectiveness at low coolant flow rates and shows no significant change at higher coolant mass flow rates, and tripod holes were better than shaped and cylindrical holes. A similar tripod hole geometry was used as one of the cases in the current study.

Besides the studies of the basic geometries above, researchers developed some complex geometries over the years. Chi et al. [16] performed geometrical optimization and experimental validation of a tripod film cooling hole with asymmetric side holes. Design of the experimental technique was used to determine an optimum tripod geometry, and it was concluded that an optimum configuration of the asymmetric tripod film hole can achieve equal to higher average film cooling effectiveness compared with a well-designed, shaped hole. Abdelmohimen [17] performed a numerical study on improving compound angle film hole performance by adding secondary branches to the main hole. He reported a maximum enhancement in overall film cooling effectiveness of about 208% at a blowing ratio of 2 due to the addition of the secondary holes. Park et al. [18] studied film cooling effectiveness of three antivortex hole geometries at three mainstream turbulence levels. Their conclusion was that all antivortex film hole cases showed higher film cooling effectiveness than the cylindrical hole, and as the mainstream turbulence intensity increased, the film

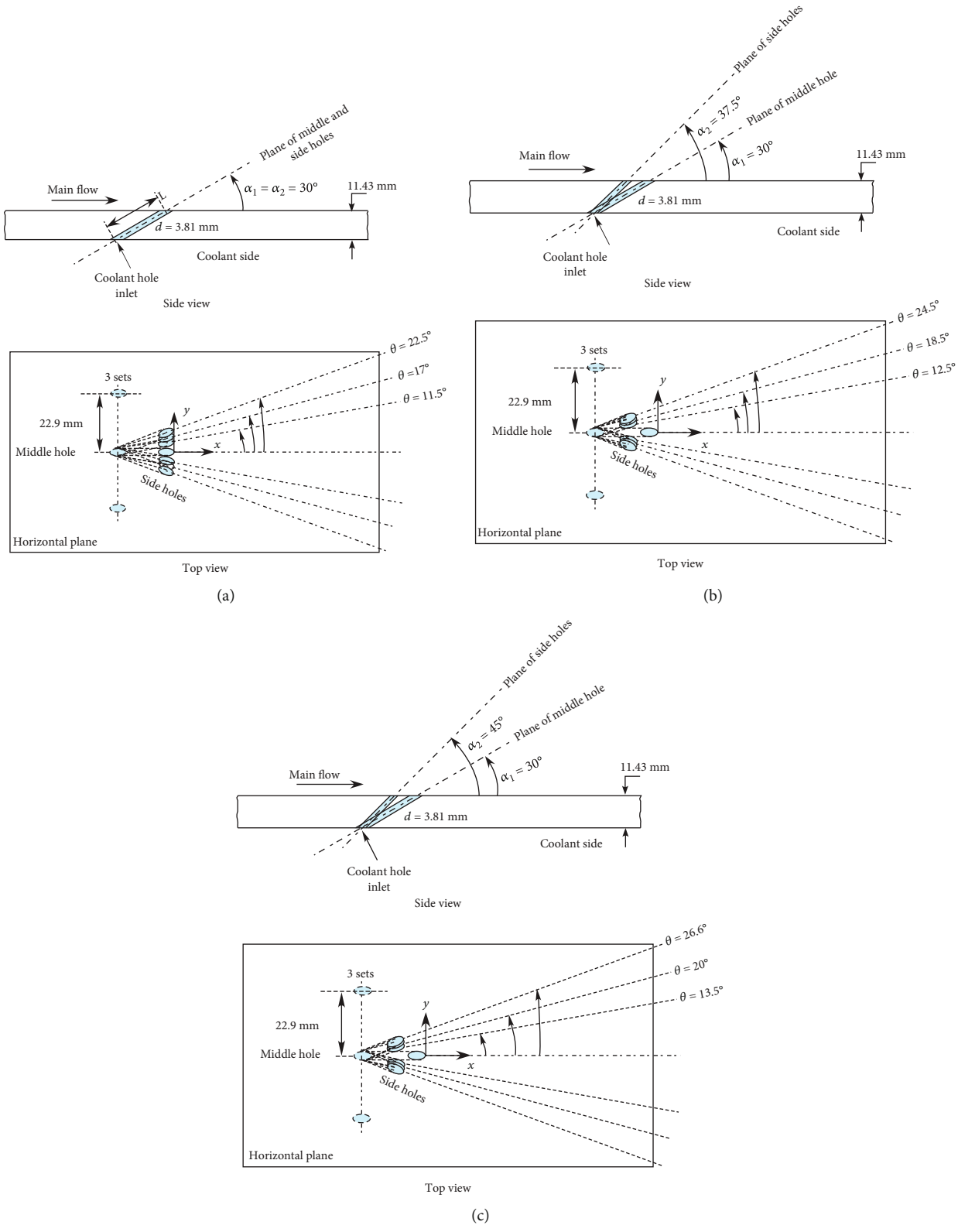

Figure 4: Details of the film cooling hole geometries. (a) Case of the three holes with the same inclination angle of 30°. (b) Case of middle (primary) hole with an inclination angle of 30° and the two side holes with an inclination angle of 37.5°. (c) Case of middle (primary) hole with an inclination angle of 30° and the two side holes with an inclination angle of 45°.

Figure 5: A typical CNC-machined test piece before testing.

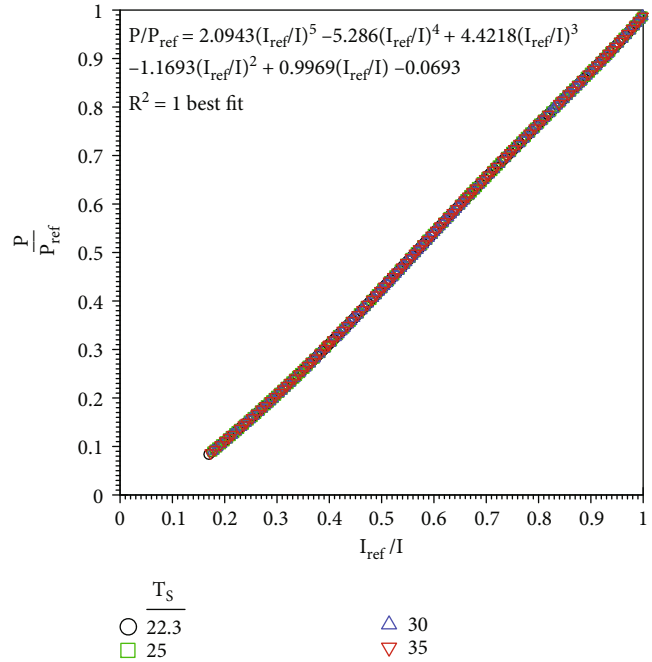

Figure 6: Calibration curve at different temperatures: 22.3, 25, 30, and 35°C.

cooling effectiveness for the antivortex holes decreased. They also showed that, among the tested hole configurations, the antivortex hole with a 15° angle between the primary and auxiliary holes had the highest film cooling effectiveness at all tested conditions.

Recent studies such as Zhu et al. [19], Cao et al. [20], Kiani and Mazaheri [21], Al-Zurfi et al. [22], Zhou et al. [23], Grine et al. [24], Al-Zurfi et al. [25], Mazaheri et al. [26], Naidu et al. [27], and Balaji et al. [28] reported on the film effectiveness results of tripod or sister antivortex holes on flat or curved surfaces. Positions and diameters of the side holes are the two key parameters that affect the overall performance at a given blowing ratio. Major conclusion of these investigations was that with the increase of the blowing ratio, the film cooling effectiveness in tripod or sister antivortex holes increases.

Schroeder and Thole [29] measured adiabatic film cooling effectiveness values for a shaped film cooling hole with an inclination angle of 30°, expansion angles in the forward and lateral directions of 7°, hole length to diameter ratio of 6, hole exit-to-inlet area ratio of 2.5, and hole lateral spacing to diameter ratio of 6. For this geometry, a major conclusion was that the peak effectiveness for all the cases with different density ratios occurred near a blowing ratio of 1.5. This laidback fan-shaped film hole geometry, which is known as the "7°-7°-7° diffusion hole", is used in this investigation as our baseline with which our results are compared.

The current study focuses on the influence of the location of the tripod side holes. Primary and side holes share the same inlet. The distance between the primary and side holes exits is controlled by varying the inclination and branch angles. The ending position of side holes is changed in both streamwise and spanwise directions. Pressure-sensitive paint is used on the test surface downstream of film holes. Nitrogen is used as the coolant against the air mainstream, which creates a density ratio of 0.97. Nine geometries with different branch and inclination angles are tested for the blowing ratios of 0.5, 1, 1.5, and 2. The results are compared with the baseline 7°-7°-7° diffusion geometry.

2. Experimental Setup

Figure 1 shows the overall assembly of the test rig and associated accessories as well as data collection equipment. The main flow (Re = 87200) was supplied by an air compressor. The secondary flow, simulating the coolant, however, was nitrogen gas, supplied from a commercially available tank. Precision pressure dials and k-type thermocouples were used to measure the pressures and temperatures at strategic points. The experimental setup simulating the main and cooling flows is shown in Figure 2. The main channel, made with 1.27 cm thick clear acrylic plastic slabs, had a cross-section of 7.62 cm by 5.08 cm and a length of 61 cm. The two plenums were fabricated with 2.54 cm thick clear acrylic plastic slabs. A removable test plate on the main channel floor accommodated the testing of different film hole geometries. Each plenum was equipped with a honeycomb flow straightener.

3. Film Hole Test Plate

For each film hole geometry, a test piece made out of a 11.43 mm thick rectangular clear acrylic plastic with dimensions of 17.78 cm by 7.62 cm mas machined. Three film holes with a center-to-center (pitch) distance of 2.29 cm were drilled in each test plate. Table 1 shows the geometric parameters. The pertinent nondimensional parameters such as P/d and L/d are in the practical range of gas turbine hot

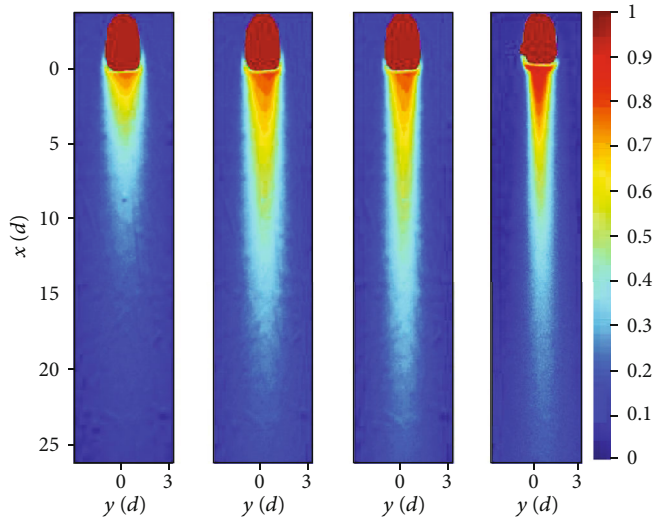

Figure 7: Film cooling effectiveness distributions downstream of the baseline geometry.

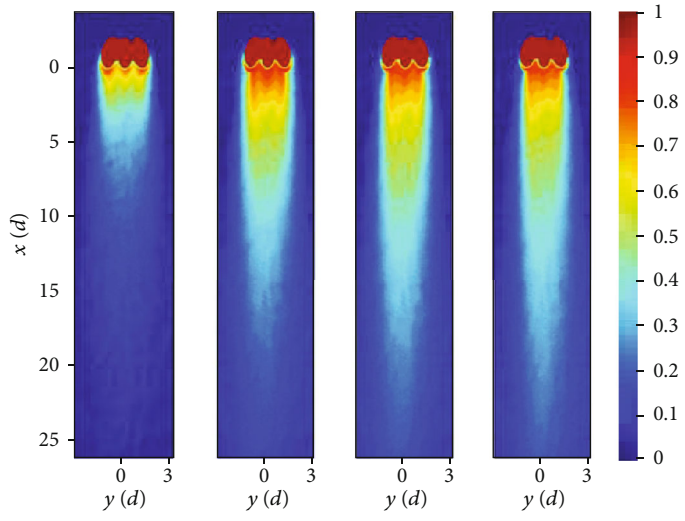

Figure 8: Film cooling effectiveness distributions downstream of the branched holes, $\alpha_2 = 30^\circ$, $\theta = 11.5^\circ$.

section designs. The baseline film hole geometry with which all proposed new geometries were compared was a 7°-7°-7° diffusion hole shown in the bottom of Figure 3. Nine sets of branched-hole geometries, each made of a 3.81 mm diameter circular hole with an inclination angle of $\alpha_1 = 30^\circ$, and two side holes were tested. The three holes in each case shared the same inlet. It should be noted that all branched-hole geometries can be envisioned in space as three tripods with the angle between the primary and side holes being 10, 15, or 20 degrees, as shown on top of Figure 3. The only difference between them was the side hole inclination angles with the exit plane (30°, 37.5°, and 45°). However, for manufacturing purposes and to uniquely define the holes, we used the exit plane as the reference plane and projected all holes on that plane. The given angles in Figures 4(a)–4(c) are the projected angles on the exit plane. A combination of three inclination angles and three branch angles, shown in Figure 4, were the nine geometries that were tested. Figure 5 shows a typical machined test piece before being installed in the test rig. On each test piece, three identical hole sets were machined and the reported film effectiveness data, streamwise or spanwise, correspond to all measurements on the middle hole set to eliminate any side effects.

4. Pressure-Sensitive Paint and Calibration

The use of pressure-sensitive paint in film cooling measurements was introduced by Navarra [30]. Compared with the temperature-sensitive paint (TSP) and infrared (IR) techniques, the pressure-sensitive paint (PSP) technique showed

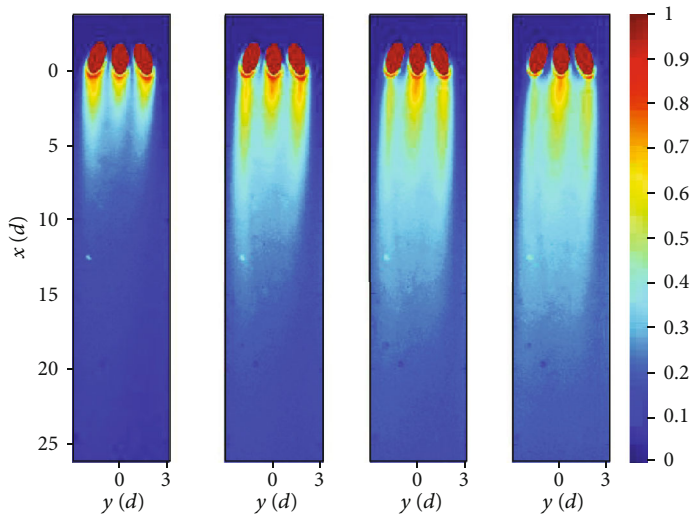

$\alpha_1 = \alpha_2 = 30°, \theta = 17°$, BR = 0.5, 1, 1.5, 2

Figure 9: Film cooling effectiveness distributions downstream of the branched holes, $\alpha_2 = 30°$, $\theta = 17°$.

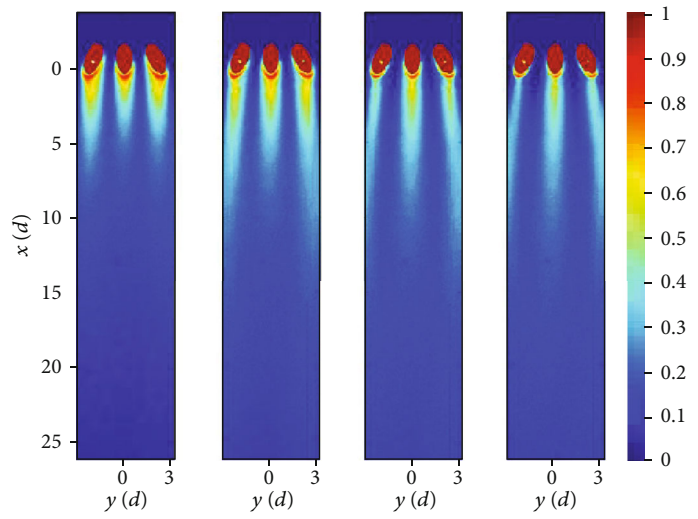

$\alpha_1 = \alpha_2 = 30°, \theta = 22.5°$, BR = 0.5, 1, 1.5, 2

Figure 10: Film cooling effectiveness distributions downstream of the branched holes, $\alpha_2 = 30°$, $\theta = 22.5°$.

a remarkable improvement in measurement accuracy because the PSP method is performed under isothermal ambient conditions; thus, there is no heat transfer of any kind between the coolant and main flow to misrepresent the extracted data. The traditional method of film cooling effectiveness measurement during the past decades made use of thermocouples for their low cost, acceptable accuracy, and relative ease of installation. They were, however, limited in numbers at discrete points and could not produce a continuous thermal image of the target surface. Furthermore, the experimentalists often had to deal with large numbers of leads passing through the target surface and take into account the conduction heat loss through the thermocouple wires. In contrast, a continuous image of the light intensity (film cooling effectiveness) of the entire surface under investigation is recorded in the PSP technique. This special paint compound is sensitive to the partial pressure of oxygen in the air-coolant mixture. When a UV light source is cast on the painted surface, the paint illuminates with varying intensity depending on the surrounding oxygen partial pressure. This property of the paint is exploited to measure the film cooling effectiveness. The analogy between the mass and energy transport equations under identical boundary conditions reveals that film cooling effectiveness can be recast into

$$\eta = \frac{C_{aw} - C_{\infty}}{C_c - C_{\infty}} = 1 - \frac{1}{1 + \left(\left(P_{O_2,air}/P_{O_2,mix}\right) - 1\right)\left(M_{N_2}/M_{air}\right)}. \quad (1)$$

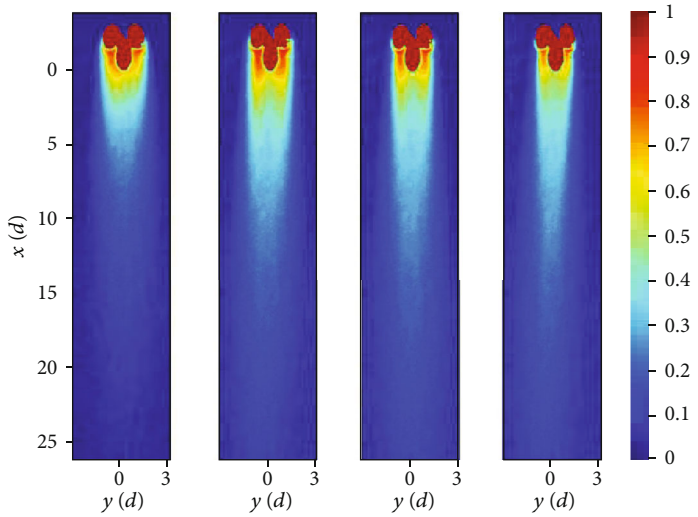

$\alpha_1 = 30°, \alpha_2 = 37.5°, \theta = 12.5°$, BR = 0.5, 1, 1.5, 2

Figure 11: Film cooling effectiveness distributions downstream of the branched holes, $\alpha_2 = 37.5°$, $\theta = 12.5°$.

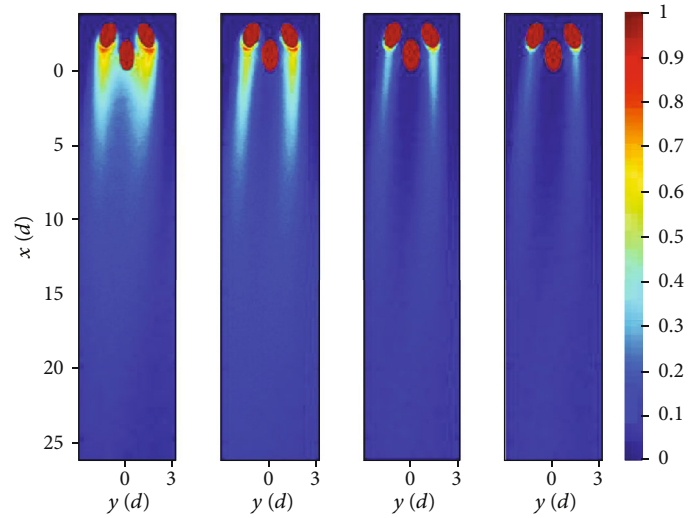

$\alpha_1 = 30°, \alpha_2 = 37.5°, \theta = 18.5°$, BR = 0.5, 1, 1.5, 2

Figure 12: Film cooling effectiveness distributions downstream of the branched holes, $\alpha_2 = 37.5°$, $\theta = 18.5°$.

The intensity ratio, which is a function of the oxygen partial pressure, can be modelled as

$$\mathrm{IR} = \frac{I_{\mathrm{ref}} - I_{\mathrm{black}}}{I - I_{\mathrm{black}}} = f\left(\frac{P}{P_{\mathrm{ref}}}\right) = f\left(P_{O_2}\right). \quad (2)$$

In this study, we used UniFIB™ pressure-sensitive paint with a FIB (fluoro/isopropyl/butyl) basecoat, acquired from the ISSI Innovative Solutions, Inc. The paint has been optimized to provide a maximum luminescence signal while it maintains high pressure sensitivity and low temperature sensitivity, which is a quality that is of prime importance in our experiments.

Before the start of the film cooling effectiveness tests, the pressure-sensitive paint was calibrated to identify a functional relation between the luminescence and partial pressure of the oxygen. A small test piece, sprayed with the same paint following the manufacturer's procedure, was placed in a sealed chamber connected to a vacuum pump. Air pressure inside the enclosure was reduced from the atmospheric pressure (101.3 kPa) to about 3 kPa. Five thermocouples at different locations measured the temperature inside the chamber. A precision vacuum gauge measured the pressure inside the compartment. Throughout the calibration process, the same lighting and camera arrangement was used to excite and record the light intensity on the test piece. The calibration

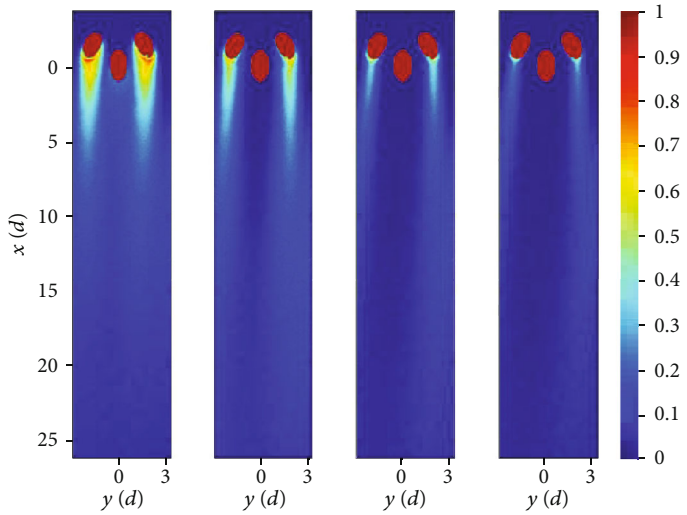

$\alpha_1 = 30°, \alpha_2 = 37.5°, \theta = 24.5°$, BR = 0.5, 1, 1.5, 2

Figure 13: Film cooling effectiveness distributions downstream of the branched holes, $\alpha_2 = 37.5°$, $\theta = 24.5°$.

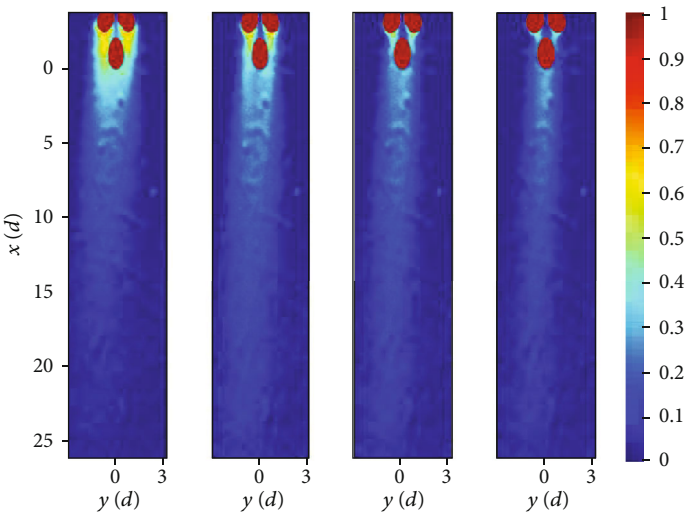

$\alpha_1 = 30°, \alpha_2 = 45°, \theta = 13.5°$, BR = 0.5, 1, 1.5, 2

Figure 14: Film cooling effectiveness distributions downstream of the branched holes, $\alpha_2 = 45°$, $\theta = 13.5°$.

test was repeated for four different test piece temperatures of 22.3, 25, 30, and 35°C. Details of the calibration setup are given in Baldino and Taslim [31]. The results from the calibration tests, shown in Figure 6, indicate that the functional dependence of luminescence with the partial pressure of oxygen remained the same in that range of surface temperature. The 5th-degree polynomial (Figure 6) representing the best fit to the data was used throughout this study to determine the film cooling effectiveness.

5. Film Cooling Effectiveness Tests

For a given film hole geometry, a typical test started with setting the targeted main flow (air) without any coolant flow, adjusting for proper lighting on the target surface and focusing the camera. Once the system reached equilibrium, a baseline photo was captured to serve as the reference light intensity to which all captured photos during a film cooling effectiveness test were compared. The next step was to turn the cooling flow (nitrogen) on and set the blowing ratio, $\mathrm{BR} = (\rho U)_{N_2}/(\rho U)_{\mathrm{air}} = (\dot{m}_{N_2}/(\pi/4)d^2)/(\dot{m}_{\mathrm{air}}/A_{\mathrm{channel}})$, to the targeted value. It should be noted that two critical flow venturies (choked at all conditions) measured the main and cooling flow mass flow rates. These mass flow rates were then divided by the main channel and the film hole inlet cross-sectional areas to determine the $(\rho U)_{\mathrm{air}}$ and $(\rho U)_{N_2}$, respectively. This procedure was consistently followed for all tested geometries. According to the pressure gauge data

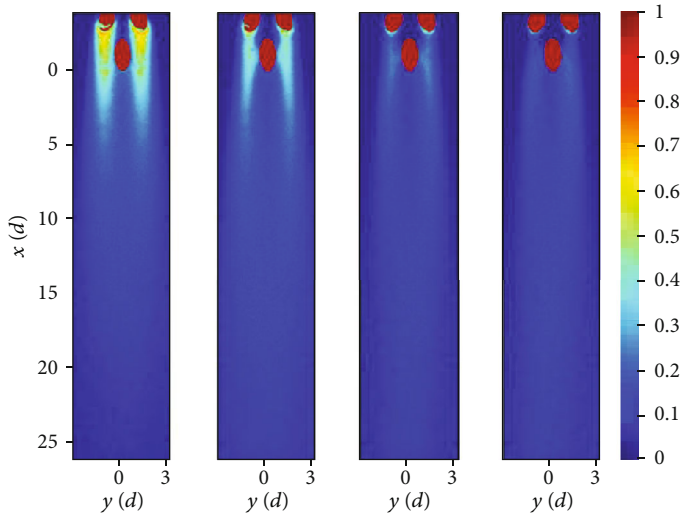

Figure 15: Film cooling effectiveness distributions downstream of the branched holes, $\alpha_2 = 45°$, $\theta = 20°$.

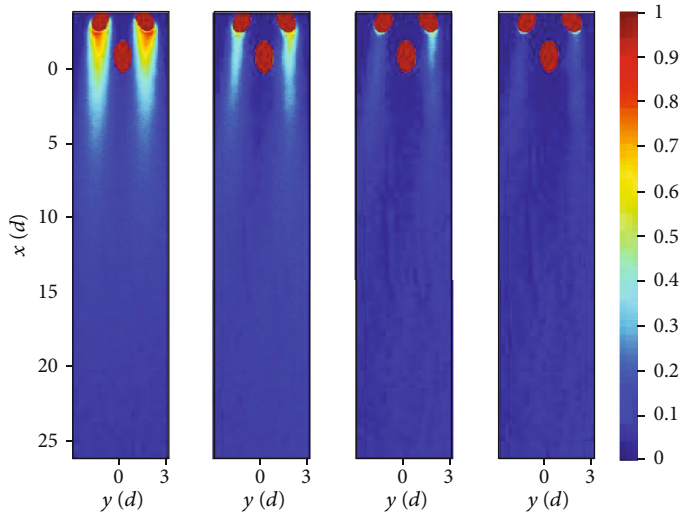

Figure 16: Film cooling effectiveness distributions downstream of the branched holes, $\alpha_2 = 45°$, $\theta = 26.5°$.

sheet, the accuracy of the device depends on the measured pressure. The maximum uncertainty in film cooling effectiveness, following the method of Kline and McClintock [32], was calculated to be about ±5%. Details of the uncertainty analysis are discussed in Baldino and Taslim [31]. The freestream turbulence intensity in the main channel was measured to be 3.86%.

6. Results and Discussion

The experiment was conducted at the constant temperature of 72 F (22.2°C). Figures 7 through 16 show the film cooling effectiveness contours for the baseline case and the nine branched-hole geometries for a range of blowing ratios. For each geometry, the blowing ratio increases from left to right corresponding to the values from 0.5 to 2, respectively. The slight tilt of the contours to the left is attributed to the machining tolerances. A visual comparison of these geometries shows that when the side and main holes have the same inclination angle of 30° ($\alpha_1 = \alpha_2 = 30°$, Figures 8–10), better coverage is achieved. In particular, when the side holes make a 17° angle with the main hole for the blowing ratio of 1.5 to 2 (Figure 9), the streamwise and spanwise distributions of coolant on the target area is superior to all other geometries including the 7°-7°-7° diffusion hole baseline case i.e., for the same amount of coolant, a branch of three circular

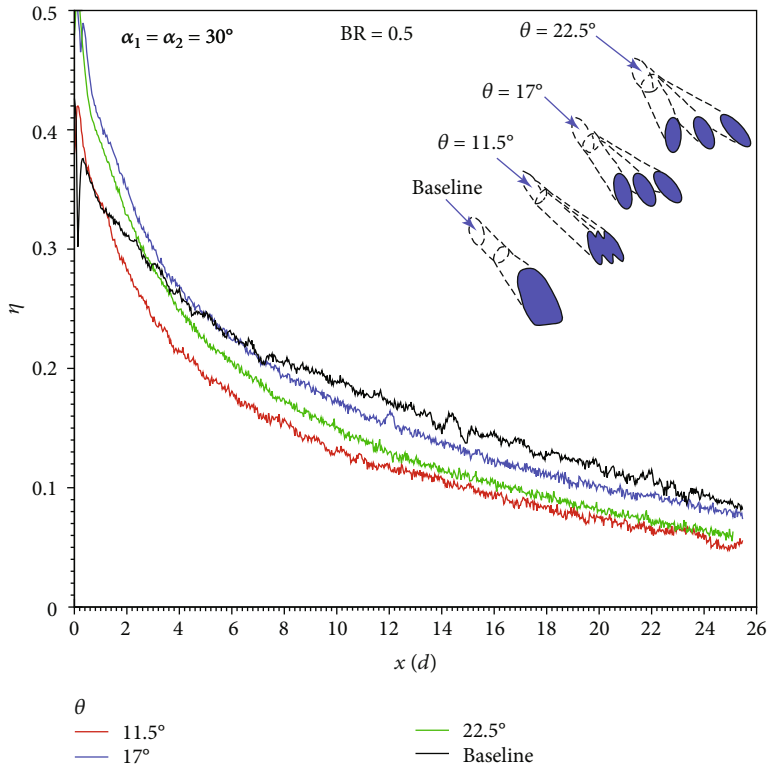

Figure 17: Streamwise (laterally averaged) film effectiveness variations for $\alpha_1 = \alpha_2 = 30^\circ$ and different branch angles for blowing ratio of BR = 0.5.

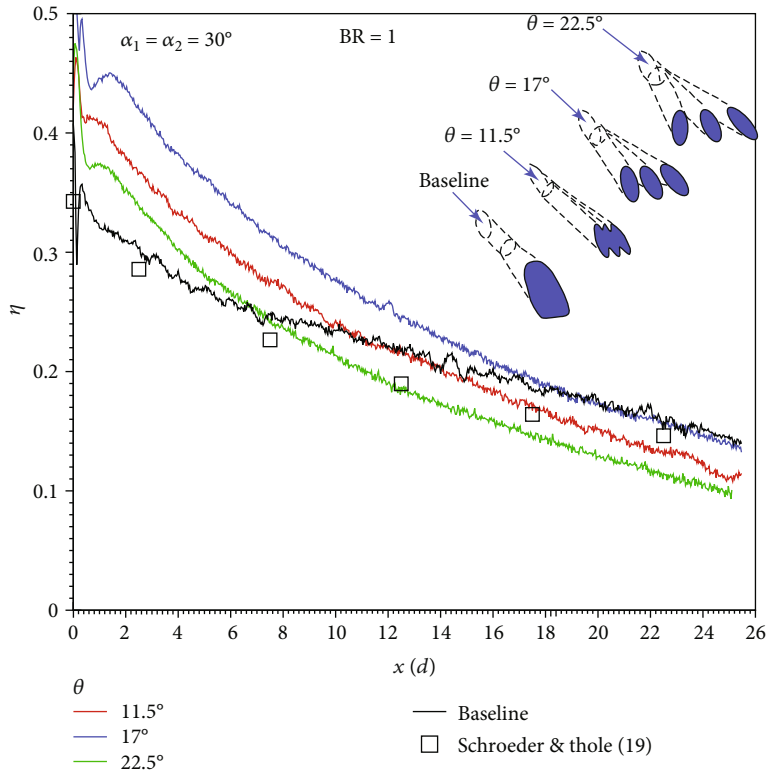

Figure 18: Streamwise (laterally averaged) film effectiveness variations for $\alpha_1 = \alpha_2 = 30^\circ$ and different branch angles for blowing ratio of BR = 1.

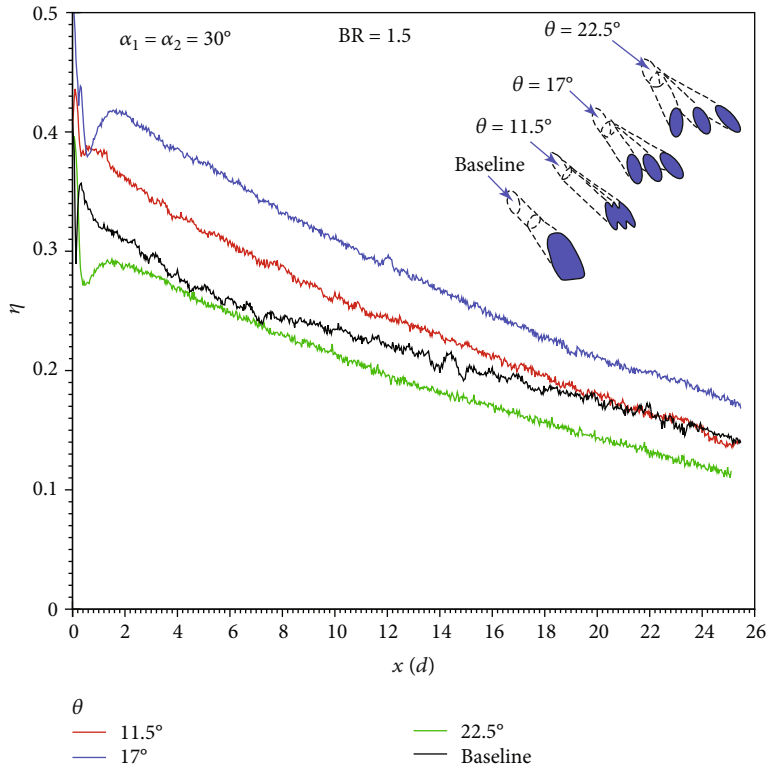

Figure 19: Streamwise (laterally averaged) film effectiveness variations for $\alpha_1 = \alpha_2 = 30°$ and different branch angles for blowing ratio of BR = 1.5.

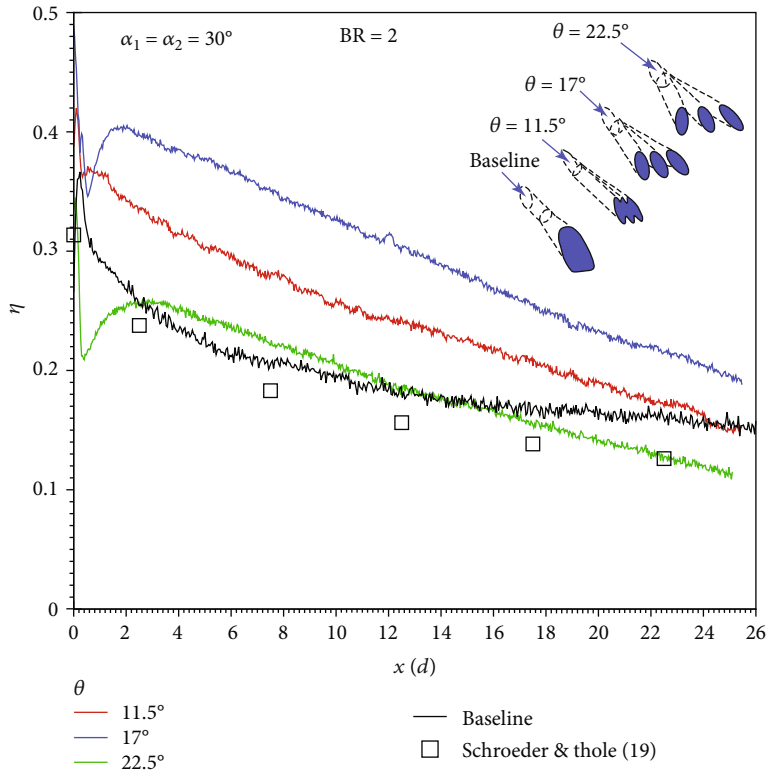

Figure 20: Streamwise (laterally averaged) film effectiveness variations for $\alpha_1 = \alpha_2 = 30°$ and different branch angles for blowing ratio of BR = 2.0.

Table 2: Area-averaged film effectiveness for $x/d = 0$-25, $y/d = -3$ to +3.

$\alpha_1 = \alpha_2 = 30^\circ$	BR = 0.5	BR = 1.0	BR = 1.5	BR = 2.0
$\theta = 11.5^\circ$	0.1396	0.2326	0.2489	0.2475
$\theta = 17^\circ$	0.1794	0.2661	0.2902	0.3025
$\theta = 22.5^\circ$	0.1591	0.2067	0.1998	0.1888
Baseline	0.1828	0.2369	0.2233	0.1973

holes performs better than the 7°-7°-7° diffusion hole. As for the manufacturing of these holes, the three circular holes are easier to laser drill than the shaped holes. As the side hole inclination angle increases to 37.5° and 45°, the film cooling effectiveness distribution deteriorates with the lowest effectiveness exhibited for $\alpha_2 = 45^\circ$, $\theta = 26.5^\circ$ and blowing ratio of 2 (Figure 16). The combination of large inclination angle and large blowing ratio causes lift-off of the coolant.

Film effectiveness contours of Figures 11–13 show that most of the coolant exits from the side holes and the film coverage deteriorates as the blowing ratio increases. The side and primary holes share the same inlet, and the coolant makes no turn entering the side holes. With the longer primary hole, the pressure gradient becomes larger in the primary hole. This explains the larger mass flow rate fraction in the side holes. We were not able to measure the coolant mass flow rate through individual holes. However, we performed a visual strings test to confirm that the side hole mass flow rate was greater than that in the primary hole for those cases that the flow footprints on the PSP showed this imbalance. As the side holes are further inclined to $\alpha_2 = 45^\circ$, the film coverage is further reduced, as shown in Figures 14–16. Again, not much coolant finds its way through the primary hole and better film coverage is evidenced for the smallest blowing ratio of 0.5 for the three branch angles.

Figures 17–20 show the laterally averaged streamwise variation of film cooling effectiveness downstream of selected film hole geometries. The cases of $\alpha_1 = \alpha_2 = 30^\circ$ are compared with the baseline case for their high performance and hole interactions according to the contours. It should be noted that the film effectiveness at each streamwise location is the spanwise-averaged film cooling effectiveness along a horizontal line drawn on the area downstream of the middle set. As observed in Figure 17, the baseline case overperformed the tripod cases at the low blowing ratio of 0.5 and beyond $x/d \sim 6$. However, it gradually lost its advantage when the blowing ratio increased. For $\theta = 11.5^\circ$, as the exits of the primary and side holes are very close to each other, the geometry can be seen as a laterally diffused hole with an expansion angle of 11.5°. Because of its high expansion angle, the case of $\theta = 11.5^\circ$ was expected to produce better cooling effectiveness. The $\theta = 17^\circ$ geometry shows the highest streamwise values with a film effectiveness of about 20% at x/d of 25 in Figure 19. This performance is not observed for any other film cooing hole geometries, including the baseline shaped-hole geometry. The case of $\theta = 22.5^\circ$ with the largest distance between the primary and side holes is the typical tripod shape that is studied by other investigators [12–15]. In this geometry, the three cylindrical holes flow separately, and the cooling flows do not have many interactions. The kidney vortex strength is reduced but not as much as the case of $\theta = 17^\circ$. The 7°-7°-7° diffusion hole data of Schroeder and Thole [29] are shown in Figures 18 and 20. Considering their measurement technique (infrared camera) and a density ratio of 1.2, the agreement is good. A noticeable advantage of these three geometries is that the area-averaged effectiveness increases with the blowing ratio, a feature that is not observed in other geometries (Table 2 below). A 3-fold exit area increase, for the same amount of coolant, reduces the coolant exit velocity, suppresses the formation of kidney vortices and consequently provides a more extended surface coverage. The overall level of film effectiveness is higher than that for the baseline case.

Cross-geometry comparisons of cases of $\alpha_1 = \alpha_2 = 30^\circ$, $\theta = 11.5^\circ, 17^\circ, 22.5^\circ$, and the baseline case are presented next in Figures 21–24. What we present is the spanwise film effectiveness variation at $x/d = 5$ across the width of the middle set. Like the streamwise distributions, the spanwise distributions for larger side hole inclination angles deteriorate due to jet lift-off at the side-hole exits and little to no flow through the middle hole. These three-hole geometries show a more uniform film coverage, compared with that of the baseline geometry which has a pointed maximum downstream of the hole exit but quickly drops to much less coverage on areas between the adjacent holes. Once again, the branch geometry with the three holes at the same inclination angle ($\alpha_1 = \alpha_2 = 30^\circ$) generated the best spanwise film coverage.

Area averaged film effectiveness for these three geometries as well as the baseline in the region $x/d = 0$ to 25, $y/d = -3$ to +3 are shown in Table 2. The case of $\theta = 17^\circ$, with interacting coolant flow from the primary and side holes, supresses the formation of kidney vortices, creates a more uniform cooling layer on the target surface, and has the best performance over all other cases at all blowing ratios.

Six more film hole geometries with side hole inclination angles of $\alpha_2 = 37.5^\circ$ and 45° were also tested. These six geometries had inferior performance compared to the four geometries discussed above due to larger inclination angles that resulted in jet lift-off. Because of space limitation, we have presented all tested geometries in Figures 25–28, each for a blowing ratio. Each color represents an inclination angle, and, within that inclination angle set, three-line thicknesses represent the three branch angles. The red color lines representing the 30° inclination angle showed the superior performance, even better film

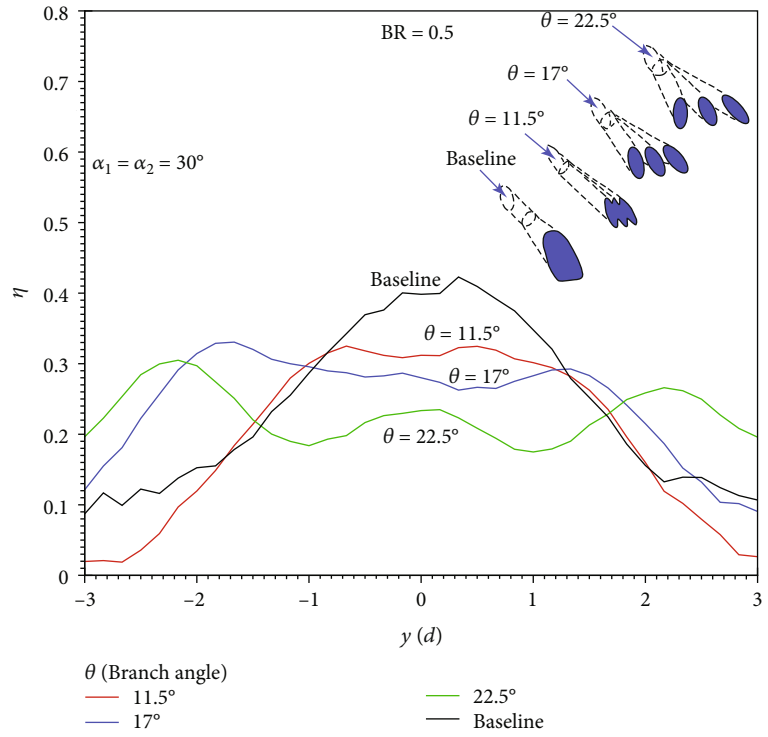

Figure 21: Spanwise (streamwise-averaged) film effectiveness variations at x/d =5 for $\alpha_{1} = \alpha_{2} = 30^{o}$ and different branch angles and blowing ratio of BR =0.5.

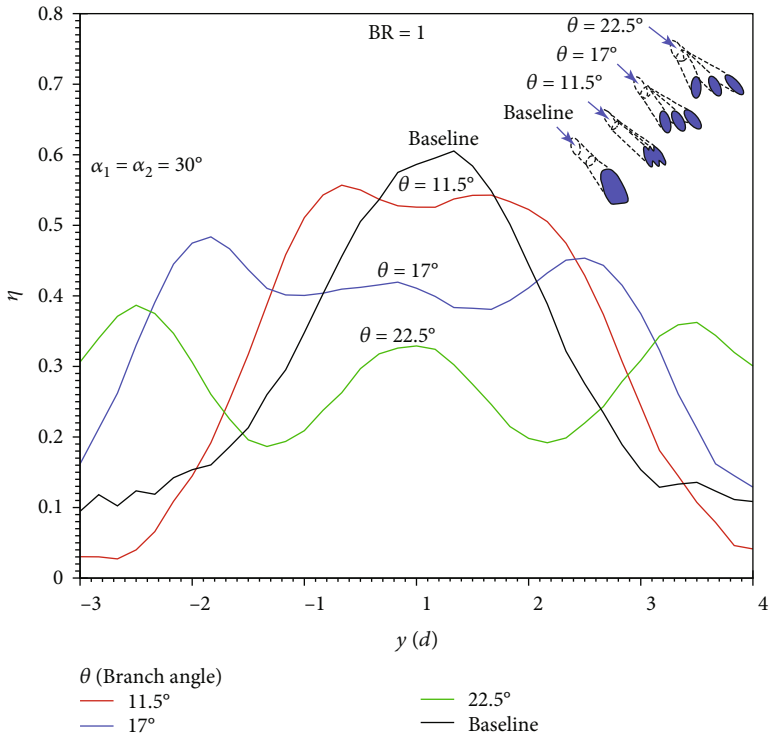

Figure 22: Spanwise (streamwise-averaged) film effectiveness variations at $x/d = 5$ for $\alpha_1 = \alpha_2 = 30^{\circ}$ and different branch angles and blowing ratio of BR = 1.

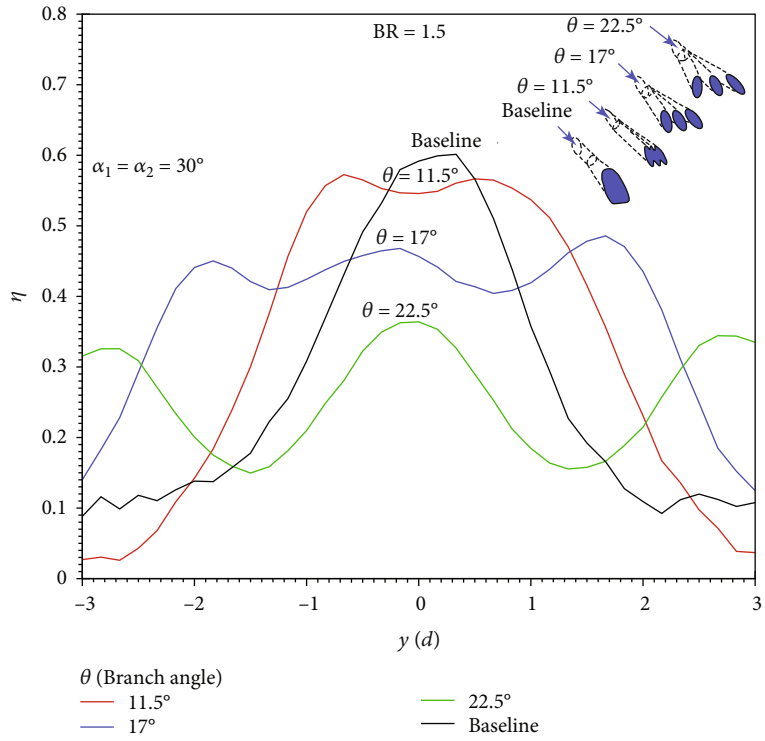

Figure 23: Spanwise (streamwise-averaged) film effectiveness variations at $x/d = 5$ for $\alpha_1 = \alpha_2 = 30^\circ$ and different branch angles and blowing ratio of BR = 1.5.

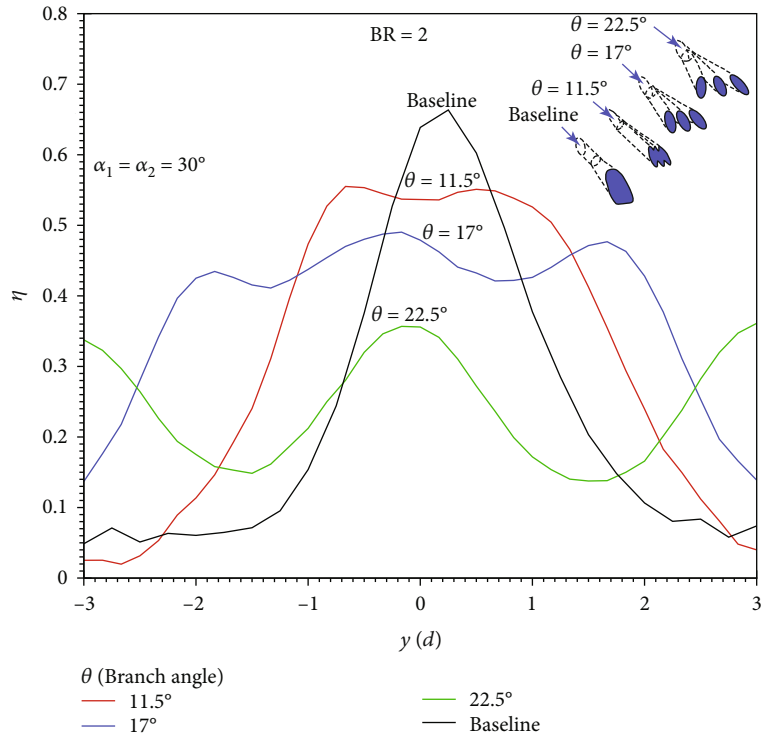

Figure 24: Spanwise (streamwise-averaged) film effectiveness variations at $x/d = 5$ for $\alpha_1 = \alpha_2 = 30^\circ$ and different branch angles and blowing ratio of BR = 2.

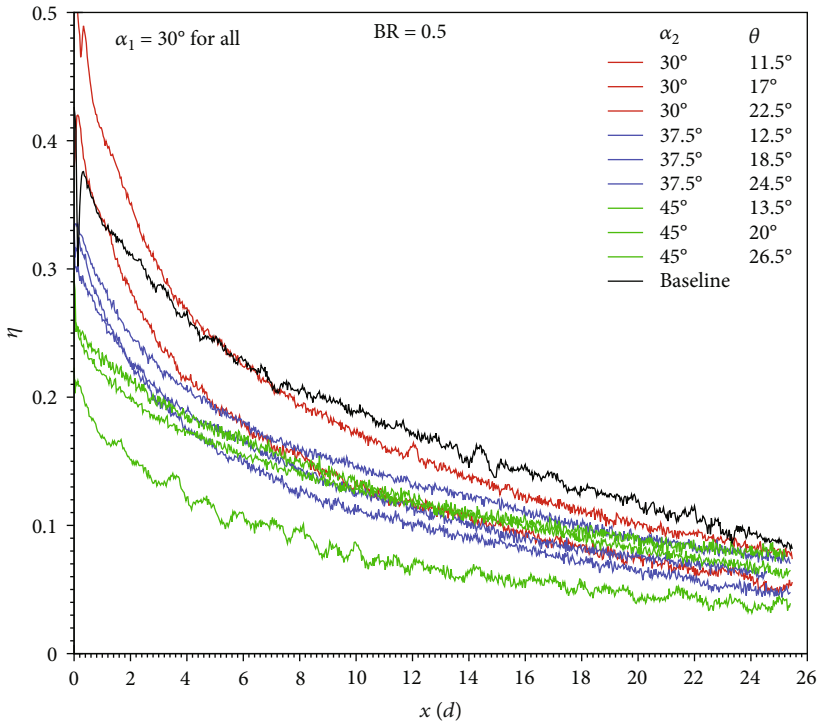

Figure 25: Comparison of streamwise (laterally averaged) film effectiveness variations for all geometries at BR = 0.5.

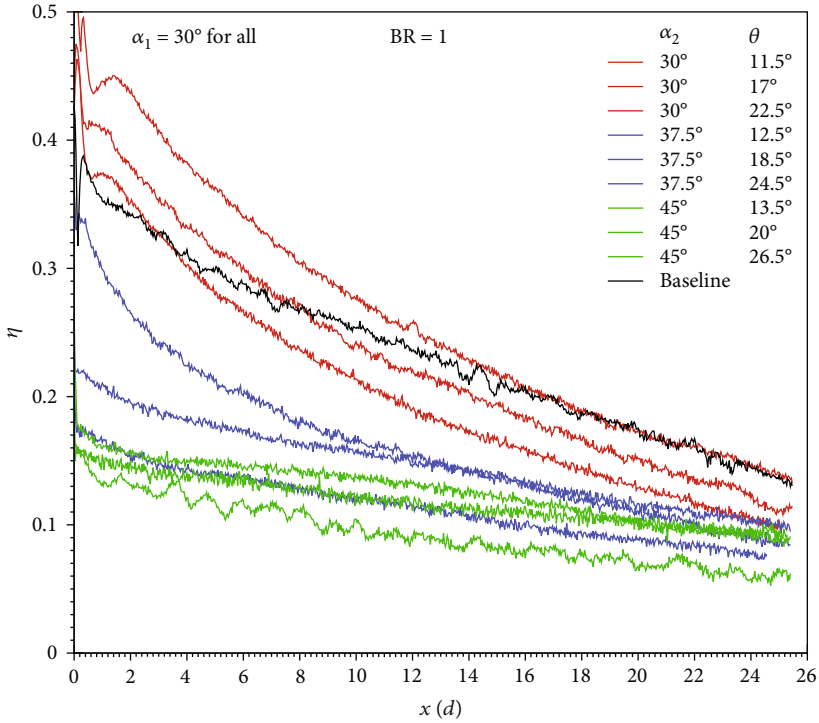

Figure 26: Comparison of streamwise (laterally averaged) film effectiveness variations for all geometries at BR = 1.

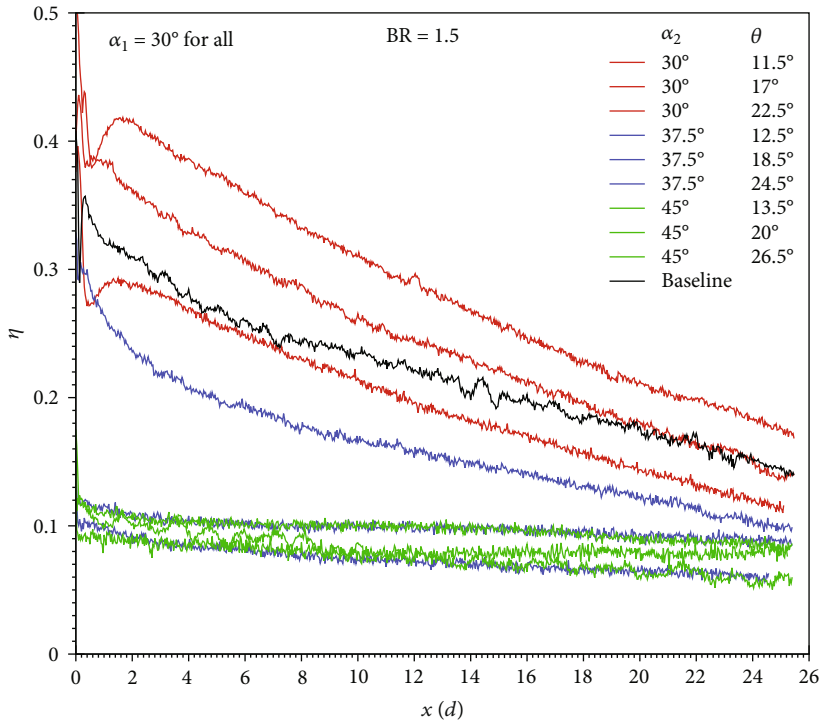

Figure 27: Comparison of streamwise (laterally averaged) film effectiveness variations for all geometries at BR = 1.5.

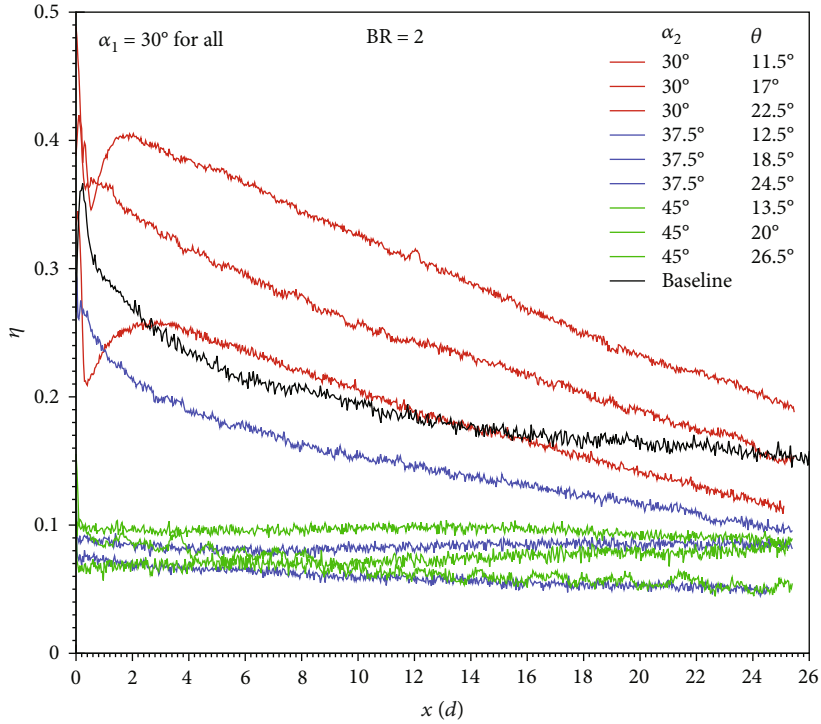

Figure 28: Comparison of streamwise (laterally averaged) film effectiveness variations for all geometries at BR = 2.

coverage than the conventional 7° -7° -7° diffusion geometry for most parts. The green color lines representing the 45° inclination angle produced the least film coverage as expected.

7. Conclusion

This study, along with the previous investigations [12–15], showed the influence of side hole locations on tripod hole film cooling. Pressure-sensitive paint was used to measure the film cooling effectiveness for nine branched hole geometries at four blowing ratios of 0.5, 1, 1.5, and 2. Major conclusions of this study are as follows: (a) branched holes with an inclination angle of 30° showed much better coverage than the 7°-7°-7° diffusion holes for all blowing ratios. Reduction in coolant velocity at the holes' exits as well as suppression of kidney vortices are believed to be responsible for this superior performance, (b) the case of main and side holes with the same inclination angle of 30°, and branch angle of 17° produced the highest film cooling effectiveness in both streamwise and spanwise directions. For this geometry, the film cooling effectiveness increased with the blowing ratio. (c) Increasing the inclination angle beyond 30° caused a remarkable decrease in film coverage.

Nomenclature

$A_{passage}$: Main flow passage area (38.71 cm^2)
BR: Blowing ratio, $(\dot{m}_{N_2}/(\pi d^2/4))/(\dot{m}_{air}/A_{passage})$
C: Chemical concentration (%)
d: Film hole inlet diameter (3.81 mm)
D_h: Main channel hydraulic diameter (60.96 mm)
I: Light intensity (pixel intensity value)
IR: The ratio of reference light intensity and measured intensity
L: Total axial length of each film hole (Figures 3 and 4)
ℓ: Feed (entrance) hole length (Figure 3, 9.53 mm)
M_c: Coolant molecular weight (28 kg/kmol)
M_∞: Mainstream (air) molecular weight (28.97 kg/kmol)
$\dot{m}_{N_2}$: Nitrogen flow rate in each tripod (kg/s)
$\dot{m}_{air}$: Main channel air mass flow rate (kg/s)
p: Hole pitch (22.86 mm)
P: Pressure (Pa)
PSP: Pressure-sensitive paint
$P_{O_2,air}$: Oxygen partial pressure in main channel approach air (Equation (1), 21 kPa)
$P_{O_2,mix}$: Oxygen partial pressure at a given point downstream the film holes (Equation (2), kPa)
Re: Reynolds number based on the main channel hydraulic diameter $((\rho U D_h/\mu) = 87200)$
TSP: Temperature-sensitive paint
U: Main channel air velocity (m/s)
α_1: Middle (primary) hole inclination angle (Figures 4)
α_2: Side hole inclination angle (Figures 4)
β_{fwd}: Shaped (diffusion) hole forward angle (Figure 3)
β_{lat}: Shaped (diffusion) hole lateral angle (Figure 3)
θ: Side holes branch angle (Figures 4)
η: Film cooling effectiveness
μ: Air dynamic viscosity (kg/(m·s))
ρ: Air density (kg/m^3).

Subscripts

aw: Adiabatic wall
blk: Black
c: Coolant
O_2: Diatomic oxygen
ref: Reference
∞: Channel mainstream.

Data Availability

Raw as well as compiled data will be available upon request.

Conflicts of Interest

The authors declare that they have no conflicts of interest.

References

[1] R. J. Goldstein, E. R. G. Eckert, and F. Burggraf, "Влияние геометрии отверстия и плотности жидкости на тріочмерное пліоночное очлаждение," *International Journal of Heat and Mass Transfer*, vol. 17, no. 5, pp. 595–607, 1974.

[2] V. L. Eriksen and R. J. Goldstein, "Heat transfer and film cooling following normal injection through a round hole," *J Eng Gas Turbine Power*, vol. 96, no. 4, pp. 329–334, 1974.

[3] D. R. Pedersen, E. R. G. Eckert, and R. J. Goldstein, "Film cooling with large density differences between the mainstream and the secondary fluid measured by the heat-mass transfer analogy," *Journal of Heat Transfer*, vol. 99, no. 4, pp. 620–627, 1977.

[4] D. G. Bogard, D. L. Schmidt, and B. Sen, "Film cooling with compound angle holes: adiabatic effectiveness," *J. Turbomachinery*, vol. 118, no. 4, pp. 807–813, 1996.

[5] B. Sen, D. L. Schmidt, and D. Bogard, "Film cooling with compound angle holes: heat transfer," *Journal of Turbomachinery*, vol. 118, no. 4, pp. 800–806, 1996.

[6] R. S. Bunker, "A review of shaped-hole turbine film-cooling technology," *J. Turbomachinery*, vol. 127, no. 4, pp. 441–453, 2005.

[7] J. Heidmann and S. V. Ekkad, "A novel antivortex turbine film-cooling hole concept," *J. turbomachinery*, vol. 130, pp. 031020-1–031020-9, 2008.

[8] A. Dhungel, Y. Lu, W. Phillips, S. V. Ekkad, and J. D. Heidmann, *Film cooling from a row of holes supplemented with anti-vortex holes*, ASME paper GT2007-27419, 2007.

[9] Y. Yao, J. Zhang, and Y. Yang, "Numerical study on film cooling mechanism and characteristics of cylindrical holes with branched jet injections," *Propulsion and Power Research*, vol. 2, no. 1, pp. 30–37, 2013.

[10] T. W. Repko, A. C. Nix, S. C. Uysal, and A. T. Sisler, "Flow visualization of multi-hole film-cooling flow under varying freestream turbulence levels," *JFCMV*, vol. 4, no. 1, pp. 13–29, 2016.

[11] S. Khajehhasani and B. A. Jubran, "Numerical assessment of the film cooling through novel sister shaped single hole schemes," *Numeri Heat Transf A Appl*, vol. 67, no. 4, pp. 414–435, 2015.

[12] C. LeBlanc, D. P. Narzary, and S. V. Ekkad, "Film-cooling performance of antivortex hole on a flat plate," *J. Turbomachinery*, vol. 135, no. 6, pp. 61009-1–61009-9, 2013.

[13] B. V. Ravi, S. Deshpande, S. Ramesh, P. D. Dhilipkumar, and S. V. Ekkad, *Film cooling performance of tripod holes on the endwall upstream of a first stage nozzle guide vane*, IMECE 2015-53133, 2015.

[14] S. Ramesh, D. G. Ramirez, S. V. Ekkad, and M. A. Alvin, "Analysis of film cooling performance of advanced tripod hole geometries with and without manufacturing features," *International Journal of Heat and Mass Transfer*, vol. 94, pp. 9–19, 2016.

[15] S. Ramesh, C. LeBlanc, D. Narzary, S. V. Ekkad, and M. A. Alvin, "Film cooling performance of tripod antivortex injection holes over the pressure and suction surfaces of a nozzle guide Vane," *J. Thermal Sci. Eng. Appl*, vol. 9, no. 2, pp. 021006-1–021006-13, 2017.

[16] Z. Chi, J. Ren, H. Jiang, and S. Zang, "Geometrical optimization and experimental validation of a tripod film cooling hole with asymmetric side holes," *J. Heat Transfer*, vol. 138, no. 6, pp. 061701-1–061701-12, 2014.

[17] M. A. H. Abdelmohimen, "Improving film cooling from compound angle holes by adding secondary holes branched out from the main holes," *Heat and Mass Transfer*, vol. 53, no. 5, pp. 1805–1815, 2017.

[18] S. S. Park, Y. J. Kim, and J. S. Kwak, "Film-cooling effectiveness of antivortex holes at three different mainstream turbulence levels," *Journal of Propulsion and Power*, vol. 33, no. 6, pp. 1561–1569, 2017.

[19] R. Zhu, E. Lin, T. Simon, and G. Xie, "Investigation and numerical simulation on film cooling performance with an anti-vortex hole design: influences of diameter ratio," *Int. Comm. Heat and Mass Transfer*, vol. 121, p. 105118, 2021.

[20] N. Cao, X. Li, Z. Wu, and X. Luo, "Effect of film hole geometry and blowing ratio on film cooling performance," *Applied Thermal Engineering, Volume*, vol. 165, p. 114578, 2020.

[21] K. C. Kiani and K. Mazaheri, "A broad reconsideration of antivortex film cooling method using numerical optimization and an improved heat-flux model," *Int. J. Heat and Fluid Flow*, vol. 89, p. 108815, 2021.

[22] N. Al-Zurfi, A. Turan, A. Nasser, and A. Alhusseny, "A numerical study of anti-vortex film-cooling holes designs in a 1-1/2 turbine stage using LES," *Propulsion and Power Research*, vol. 8, no. 4, pp. 275–299, 2019.

[23] J. Zhou, X. Wang, J. Li, and H. Lu, "Effects of diameter ratio and inclination angle on flow and heat transfer characteristics of sister holes film cooling," *Int. Comm. Heat and Mass Transfer*, vol. 110, p. 104426, 2020.

[24] M. Grine, K. Boualem, A. Z. Dellil, and A. Azzi, "Improving adiabatic film-cooling effectiveness spanwise and lateral directions by combining BDSR and anti-vortex designs," *Thermophysics and Aeromechanics*, vol. 27, pp. 749–758, 2020.

[25] N. Al-Zurfi, A. Nasser, and A. Alhusseny, "Heat transfer enhancement using an innovative film cooling design," 2019, http://iape-conference.org/Downloads/Proceedings/Proceedings%20of%20IAPE'19.pdf.

[26] K. Mazaheri, K. C. Kiani, and M. Karimi, "Application of a modified algebraic heat-flux model and second-moment-closure to high blowing-ratio film-cooling and corrugated heat-exchanger simulations," *Applied Thermal Engineering*, vol. 124, pp. 948–966, 2017.

[27] M. J. Naidu, K. Lambe, and A. Nandan, "A study on film cooling performance parameters of gas turbine blades," in *J. Analysis and Computation (JAC), http://www.ijaconline.com, ISSN 0973-2861 Int. Conf. on Knowledge Discovery in Science and Technology*, ICKDST '19, Pune, 2019.

[28] S. Balaji, F. Yang, and M. E. Taslim, "A comparative experimental study between the film effectiveness of trench and diffusion film holes," *Int. J. Heat & Mass Transfer*, vol. 161, p. 106713, 2021.

[29] R. P. Schroeder and K. A. Thole, *Adiabatic effectiveness measurements for a baseline shaped film cooling hole*, Paper # GT2014-25992, 2014.

[30] K. R. Navarra, *Development of the pressure-sensitive-paint technique for advanced turbomachinery applications*, Doctoral dissertation, Virginia Tech, 1997.

[31] F. Baldino and M. E. Taslim, *Experimental film cooling effectiveness of multi-row patterns on flat and step-down surfaces*, Paper # GT-2019-90108, 2019.

[32] S. J. Kline and F. A. McClintock, "Describing uncertainty in single-sample experiments," *Mechanical Engineering*, vol. 75, pp. 3–8, 1953.